

Article

Zinc(II) Sulfanyltribenzoporphyrazines with Bulky Peripheral Substituents—Synthesis, Photophysical Characterization, and Potential Photocytotoxicity

Patrycja Koza ^{1,2,*} , Tomasz Koczorowski ¹ , Dariusz T. Młynarczyk ¹  and Tomasz Goslinski ^{1,*} 

¹ Chair and Department of Chemical Technology of Drugs, Poznan University of Medical Sciences, Grunwaldzka 6, 60-780 Poznań, Poland; tkoczorowski@ump.edu.pl (T.K.); mlynarczykd@ump.edu.pl (D.T.M.)
² Doctoral School, Poznan University of Medical Sciences, Bukowska 70, 60-812 Poznań, Poland
* Correspondence: patrycja.koza@student.ump.edu.pl (P.K.); tomasz.goslinski@ump.edu.pl (T.G.)

Abstract: The study's aim was to synthesize new unsymmetrical sulfanyl zinc(II) porphyrazines and subject them to physicochemical and electrochemical characterization and also an initial acute toxicity assessment. The procedure was initiated from a commercially available dimercaptomaleonitrile disodium salt and o-phthalonitrile using Linstead's macrocyclization reaction conditions, which led to magnesium(II) tribenzoporphyrazine with 4-(3,5-dibutoxycarbonylphenoxy)butylthio substituents. The obtained macrocycle was demetallated with trifluoroacetic acid and subsequently remetallated with zinc(II) acetate toward the zinc(II) porphyrazine derivative. The zinc(II) tribenzoporphyrazine with 4-(3,5-dibutoxycarbonylphenoxy)butylthio substituents was then subjected to the reduction reaction with LiAlH₄, yielding zinc(II) tribenzoporphyrazine with 4-[3,5-di(hydroxymethyl)phenoxy]butylthio substituents. The new zinc(II) tribenzoporphyrazines were characterized by UV-Vis spectroscopy, various NMR techniques (¹H NMR, ¹³C NMR, ¹H-¹H COSY, ¹H-¹³C HSQC, and ¹H-¹³C HMBC), and mass spectrometry. In the UV-Vis spectra, both macrocycles revealed characteristic Soret and Q-bands, whose positions were dependent on the solvent used for the measurements. Zinc(II) tribenzoporphyrazines were studied using electrochemical and photochemical methods, including the singlet oxygen generation assessment. Both zinc(II) porphyrazines revealed high singlet oxygen generation quantum yield values of up to 0.59 in DMSO, which indicates their potential photosensitizing potential for photodynamic therapy. In addition, new derivatives were subjected to a Microtox[®] bioluminescence assay.

Keywords: acute toxicity; macrocyclization; porphyrazines; singlet oxygen generation; solvatochromic study



Citation: Koza, P.; Koczorowski, T.; Młynarczyk, D.T.; Goslinski, T. Zinc(II) Sulfanyltribenzoporphyrazines with Bulky Peripheral Substituents—Synthesis, Photophysical Characterization, and Potential Photocytotoxicity. *Appl. Sci.* **2022**, *12*, 6825. <https://doi.org/10.3390/app12136825>

Academic Editors: Carolina Belver and Maria José Fernandes Sampaio

Received: 11 May 2022

Accepted: 27 June 2022

Published: 5 July 2022

Publisher's Note: MDPI stays neutral with regard to jurisdictional claims in published maps and institutional affiliations.



Copyright: © 2022 by the authors. Licensee MDPI, Basel, Switzerland. This article is an open access article distributed under the terms and conditions of the Creative Commons Attribution (CC BY) license (<https://creativecommons.org/licenses/by/4.0/>).

1. Introduction

Synthetic analogues of naturally occurring porphyrins are porphyrazines (Pzs). The macrocyclic core of Pzs consists of four pyrrole rings linked together by azamethine bridges [1]. Pzs reveal unique spectroscopic, photochemical, and electrochemical properties that make them suitable for potential applications in technology and medicine [2–5]. The absorption of light in the range of 650–850 nm, which is often described as the phototherapeutic window, as well as the generation of reactive oxygen species in the photodynamic reaction, make Pzs especially relevant for medical applications, in particular photodynamic therapy (PDT) [6]. The PDT principle is based on the photodynamic reaction, which starts from the exposure of the photosensitizer to light of an appropriate wavelength [7]. Upon irradiation, the photosensitizer situated in a specific tumor tissue is activated from the ground singlet state to the first excited state and next, by the chain of transitions, to the triplet state. The presence of the macrocyclic molecule in its triplet state is vital for the production of reactive oxygen species (ROS), including singlet oxygen (¹O₂), further initiating apoptotic or necrotic cell death. The most commonly used photosensitizers in

PDT are porphyrins and their derivatives [8]. Nevertheless, many years of research on porphyrazines have also shown their great potential for future PDT applications.

The lipophilic properties of Pzs are particularly beneficial, as cancer cells often overexpress LDL receptors, which could increase the effectiveness of the therapy [9]. However, the lipophilic character of Pzs could also constitute the main obstacle for prospective applications of Pzs in PDT. This is because the non-polar macrocyclic core of Pzs decreases their solubility in water, thus increasing their ability to form aggregates in polar solvents, which in turn hampers their ability to produce ROS. The increase in the solubility of Pzs can be indirectly achieved by incorporating these macrocycles into different drug-delivery systems, such as liposomes [10–13] or polymers [14–17]. Nevertheless, the direct and practical possibility of solubility improvement of these compounds is possible due to the substitution of the Pz core in the peripheral positions. In this regard, sulfanyl peripheral substituents attached to the porphyrazine macrocycle can significantly enhance the solubility of these macrocycles in various solvents [18,19]. Both sulfanyl porphyrazines and tribenzoporphyrazines can be prepared using Linstead's macrocyclization reaction conditions. As stated before by our group [20], sulfanyl porphyrazines reveal low to moderate singlet oxygen generation efficacies. A tribenzoporphyrazine analogue with terminal hydroxyl groups at the periphery has presented the highest generation of singlet oxygen ($\phi_{\Delta} = 0.20$) and excellent photocytotoxicity, which can be related to its solubility and localization. Therefore, in our current study, we present the synthesis of new unsymmetrical sulfanyl zinc(II) porphyrazines, their physicochemical characterization, and an initial acute toxicity assessment.

2. Materials and Methods

2.1. General Procedures

All reactions were carried out in oven-dried glassware under an inert gas atmosphere. When needed, Radley's Heat-On heating system was used. Solvents were evaporated by using a rotary evaporator at or below 60 °C under reduced pressure. Reagents and solvents were used without purification and were obtained from commercial suppliers, i.e., Sigma-Aldrich, Fluka, POCh, and Merck. Thin-layer chromatography (TLC) was performed on silica gel Merck Kieselgel 60 F254 plates and visualized by UV light. The NMR spectra (^1H NMR, ^{13}C NMR, ^1H - ^1H COSY, ^1H - ^{13}C HSQC, and ^1H - ^{13}C HMBC) were recorded using a full-fledged, two-channel 400 MHz Bruker AvanceCore NMR spectrometer. The mass spectra were recorded using the ESI method on a Bruker Impact HD by the Wielkopolska Centre for Advanced Technologies in Poznań.

2.2. Synthetic Procedures

The precursor compounds, dimethyl 5-(4-bromobutoxy)isophthalate (1) and 2,3-bis[4-(3,5-dimethoxycarbonylphenoxy)butylsulfanyl]maleonitrile (2), and the magnesium(II) tribenzoporphyrazine derivatives, 22,23-bis[4-(3,5-dibutoxycarbonylphenoxy)butylthio]-tribenzo[b,g,l]porphyrazinato magnesium(II) (3) and 22,23-bis[4-[3,5-di(hydroxymethyl)phenoxy]butylthio]tribenzo[b,g,l]porphyrazinato magnesium(II) (4), were synthesized using previously published procedures [18,20]. Metal-free tribenzoporphyrazine 22,23-bis[4-(3,5-dibutoxycarbonylphenoxy)butylsulfanyl]tribenzo[b,g,l]porphyrazine was synthesized according to the literature procedure [21].

2.2.1. 22,23-Bis[4-(3,5-dibutoxycarbonylphenoxy)butylthio]-tribenzo[b,g,l]porphyrazinato Zinc(II) (6)

Magnesium(II) porphyrazine derivative 3 (107 mg, 0.086 mmol) was suspended in trifluoroacetic acid (5 mL) and stirred for 30 min in the dark at room temperature. The suspension was poured into an ice–water mixture, then neutralized with a saturated solution of sodium bicarbonate and extracted with dichloromethane. The organic layers were combined, the organic solvent was evaporated, and the dark blue solid residue was then subjected to column chromatography (dichloromethane/methanol 20:1) [21]. Metal-

free Pz derivative **5** (92 mg, 0.075 mmol), *N,N*-dimethylformamide (DMF, 25 mL), and zinc(II) acetate (41 mg, 0.225 mmol) were stirred in a round-bottomed flask under inert gas at 70 °C for 24 h. After that, the solvent was evaporated, and the residual blue oil was subjected to column chromatography (dichloromethane/methanol 50:1 then 20:1), leading to a cerulean blue product **6** (79 mg, 71% yield). $R_f = 0.71$ (dichloromethane/methanol, 20:1, *v/v*). UV-Vis (dichloromethane) λ_{\max} nm (log ϵ) 227 (4.84), 352 (4.69), 649 (4.73), 692 (4.89). ^1H NMR (400 MHz, pyridine- d_5) δ 9.65–9.70 (m, 4H, tribenzo-*H*), 9.58 (2d, $J = 8$ Hz, 2H, tribenzo-*H*), 8.31 (s, 2H, isophthalate-*H*), 8.26 (2d, $J = 5.5$ Hz, 2H, tribenzo-*H*), 8.18–8.23 (m, 4H, tribenzo-*H*), 7.55 (s, 4H, isophthalate-*H*), 4.67 (t, $J = 7$ Hz, 4H, PhOCH_2), 4.22 (t, $J = 7$ Hz, 8H, C(O)OCH_2), 4.00 (t, $J = 6$ Hz, 4H, SCH_2), 2.26–2.39 (m, 8H, $\text{SCH}_2\text{CH}_2\text{CH}_2$), 1.48–1.55 (m, 8H, $\text{CH}_2\text{CH}_2\text{CH}_3$), 1.22–1.31 (m, 8H, CH_2CH_3), 0.79 (t, $J = 7$ Hz, 12H, CH_3). ^{13}C NMR (101 MHz, pyridine- d_5) δ 165.7 (C = O), 159.6, 158.3, 157.8, 154.4, 153.5, 140.3, 140.1, 139.4, 138.7, 132.6, 131.1, 130.9, 130.4, 119.8, 68.3 (SCH_2CH_2), 65.6 ($\text{OCH}_2\text{CH}_2\text{CH}_2\text{CH}_3$), 35.7 ($\text{CH}_2\text{CH}_2\text{O}$), 31.1 ($\text{CH}_2\text{CH}_2\text{CH}_3$), 28.9 ($\text{SCH}_2\text{CH}_2\text{CH}_2$), 27.8 ($\text{SCH}_2\text{CH}_2\text{CH}_2$), 19.7 (CH_2CH_3), 14.1 (CH_3). MS (ESI): m/z : calcd. ($\text{C}_{68}\text{H}_{71}\text{N}_8\text{O}_{10}\text{S}_2\text{Zn}$): 1287.4020 [$\text{M} + \text{H}$] $^+$, found: 1287.4015.

2.2.2. 22,23-Bis{4-[3,5-di(hydroxymethyl)phenoxy]butylthio}tribenzo[b,g,l]porphyrazinato Zinc(II) (**7**)

Lithium aluminum hydride (13 mg, 0.353 mmol) was suspended in tetrahydrofuran (THF) precooled to 0 °C and stirred for 30 min. Porphyrazine derivative **6** (95 mg, 0.074 mmol) was dissolved in THF (14 mL), and the solution was added dropwise to the reaction mixture over 40 min. Next, the combined reagents were stirred for another 2 h at room temperature. After that, the saturated solution of NH_4Cl (5 mL) was added, and the reaction mixture was stirred for 15 min. The reaction mixture was filtered through Celite, which was additionally washed with dichloromethane. Next, all solvents were evaporated to dryness using a rotary evaporator. Peacock blue residue was chromatographed (dichloromethane/methanol 20:1) to give **7** (67 mg, 90% yield) as a dark sapphire blue film. $R_f = 0.62$ (dichloromethane/methanol, 20:1, *v/v*). UV-Vis (dichloromethane) λ_{\max} nm (log ϵ) 227 (4.76), 358 (4.59), 629 (4.45), 725 (4.55). ^1H NMR (400 MHz, pyridine- d_5) δ 9.46–9.58 (m, 4H, tribenzo-*H*, isophthalate-*H*), 8.19–8.41 (m, 6H, tribenzo-*H*, isophthalate-*H*), 7.35–7.67 (m, 6H, tribenzo-*H*, isophthalate-*H*), 4.18–4.26 (s, 4H, OCH_2CH), 2.15–2.42 (m, 4H, SCH_2CH_2), 1.48–1.55 (m, 4H, $\text{SCH}_2\text{CH}_2\text{CH}_2$), 1.20–1.34 (m, 4H, $\text{SCH}_2\text{CH}_2\text{CH}_2$), 0.90–0.97 (m, 8H, CH_2OH). ^{13}C NMR (101 MHz, pyridine- d_5) δ 165.8, 165.5, 159.7, 140.3, 132.8, 132.4, 123.0, 124.5, 122.5, 122.7 119.9, 119.5, 67.8 (SCH_2), 53.7 (CH_2O) 31.1 (SCH_2CH_2), 19.7, 14.2 (CH_2OH). MS (ESI): m/z calcd. ($\text{C}_{52}\text{H}_{47}\text{N}_8\text{O}_6\text{S}_2\text{Zn}$): 1007.2346 [$\text{M} + \text{H}$] $^+$, found: 1007.2351.

2.3. UV/Vis Measurements

All solutions containing macrocycles **6** and **7** were prepared before their absorbance measurements. UV-Vis absorption spectra were recorded using a JASCO 770 spectrophotometer in the wavelength range from 190 to 800 nm. Solvatochromic studies were collected in 12 solvents: dichloromethane (DCM), chloroform, acetone, diethyl ether, ethyl acetate, acetonitrile, 1,4-dioxane, THF, 1-butanol, toluene, dimethyl sulfoxide (DMSO), and DMF using the same quantity of either **6** or **7** in each solvent.

2.4. Electrochemical Measurements

Electrochemical experiments were performed with a Metrohm Autolab PGSTAT128N potentiostat connected to a PC for data acquisition and storage, driven by Metrohm Nova 2.1.4 software. The setup for organic measurements in dichloromethane consisted of the glassy carbon (GC) working electrode (area = 0.071 cm 2), an Ag wire as the pseudo-reference electrode, and a platinum wire as the counter electrode. Before each experiment, the GC electrode was polished with an aqueous 50 nm Al_2O_3 slurry (provided by Sigma-Aldrich, St. Louis, MI, USA) on a polishing cloth, followed by subsequent washing in an ultrasonic bath with deionized water for 10 min in order to remove inorganic impurities. A ferrocene-

nium/ferrocene couple (Fc^+/Fc) was used as an internal standard. Before the experiments, a glass cell (volume 10 mL) containing the solution sample with a supporting electrolyte (0.1 M tetrabutylammonium perchlorate, TBAP) was deoxygenated by purging nitrogen gas. All electrochemical experiments were carried out at ambient laboratory temperature. DCM and TBAP were purchased from Sigma-Aldrich.

2.5. Singlet Oxygen Generation Study

A singlet oxygen generation study was performed following the previously described method [22]. 1,3-Diphenylisobenzofuran (DPBF) was applied as a chemical quencher (Sigma-Aldrich) for singlet oxygen generation measurements. New porphyrazines 6–7 and the quencher were exposed to light at the appropriate wavelength (665 nm) and examined by UV-Vis. As a reference, zinc(II) phthalocyanine (ZnPc) was used with a known singlet oxygen quantum yield (0.67 in DMSO) [23,24].

2.6. Acute Toxicity Assessment

The acute toxicity test for the dark toxicity assessment was performed following the 81.9% screening test procedure supplied by the manufacturer and measured with a Microtox[®] M500 with Modern Water MicrotoxOmini 4.2 software. The tested macrocycles were dissolved in DMSO and diluted to the appropriate concentrations with water. The DMSO concentration was lower than 1%, which was confirmed not to interfere with the results.

The photocytotoxicity was evaluated by slightly modifying the procedure [25]. Upon the addition of the sample to the bacterial suspension, an LED lamp was placed above the test cuvettes ($\lambda_{\text{max}} = 665 \text{ nm}$, 7 mW/cm^2).

3. Results and Discussion

3.1. Synthesis and Characterization

In the first step, commercially available dimercaptomaleonitrile disodium salt and *o*-phthalonitrile were applied to Linstead's macrocyclization reaction conditions, which led to magnesium(II) tribenzoporphyrazine with 4-(3,5-dibutoxycarbonylphenoxy)butylthio substituent 3 (Scheme 1) [26,27]. This macrocycle was subjected to the reduction reaction with LiAlH_4 , which led to magnesium(II) tribenzoporphyrazine with 4-[3,5-di(hydroxymethyl)phenoxy]butylthio substituents 4 [28]. Tribenzoporphyrazine derivatives 3 and 4 were obtained according to the previously published procedure and purified using flash column chromatography [20]. Macrocycle 3 was treated with trifluoroacetic acid, leading to the demetallated derivative [21] and then was subsequently remetallated with zinc(II) acetate toward zinc(II) tribenzoporphyrazine with 4-(3,5-dibutoxycarbonylphenoxy)butylthio substituent 6. Next, Pz 6 was subjected to the reduction reaction with LiAlH_4 , which allowed zinc(II) tribenzoporphyrazine with 4-[3,5-di(hydroxymethyl)phenoxy]butylthio substituents 7 to be obtained. The new zinc(II) tribenzoporphyrazines 6 and 7 were characterized using UV-Vis spectroscopy, various NMR techniques (^1H NMR, ^{13}C NMR, ^1H - ^1H COSY, ^1H - ^{13}C HSQC, and ^1H - ^{13}C HMBC), and mass spectrometry. The NMR data concerning the analysis of chemical shifts and key observed correlations are included in the Supplementary Materials.

3.2. Absorption Properties of New Porphyrazines

As was stated by C. F. van Nostrum et al., the metal ions in the coordination centers and the peripheral substituents strongly influence the electronic absorption spectra of the porphyrinoids [29]. In general, in the spectra of Pzs, two characteristic bands can be observed, the Soret band (B-band) in the range of 300–400 nm and the Q-band in the range of 600–850 nm [29–32]. The Q-bands that appeared in the spectra of both Pzs 6 and 7 recorded in different solvents are presented in Figure 1. Following the data presented in Table 1, the Soret maxima of 6 and 7 appeared in the ranges of 337–361 and 338–366 nm, whereas the Q-bands were present in the ranges of 681–701 and 682–723 nm, respectively.

The Q-band positions reflect the effects of π - π^* electron transitions from HOMO (highest occupied molecular orbital) to LUMO (lowest unoccupied molecular orbital) and constitute a characteristic feature of the studied macrocycles. The Q-bands of obtained Pzs **6** and **7** are split into two components, Q_x and Q_y , which could result more from their decreased symmetry than the formation of aggregates. The Soret-band position is also a consequence of π - π^* transitions but from the molecular orbital (MO) to LUMO. The slight modifications of the **6** and **7** peripheries as well as the solvent choice significantly affected the positions of the B- and Q-bands in the UV-Vis spectra. The main difference was the distances between the Q_x and Q_y components of the Q-bands form, which were approximately 43 nm for **6** and 94 nm for **7** in dichloromethane. In addition, peripheral sulfur atoms could also influence the photophysics of both Pzs. Following the literature, in the magnesium(II) octacarboranyl(hexylsulfanyl)porphyrazine UV-Vis spectra, an additional absorption band at approximately 500 nm was noted as a result of $n_{\text{sulfur}}-\pi^*$ transitions [33]. Such phenomena were noted in the spectra of **6** measured in DCM and ethyl acetate and in the spectra of **7** recorded in DCM and acetonitrile.

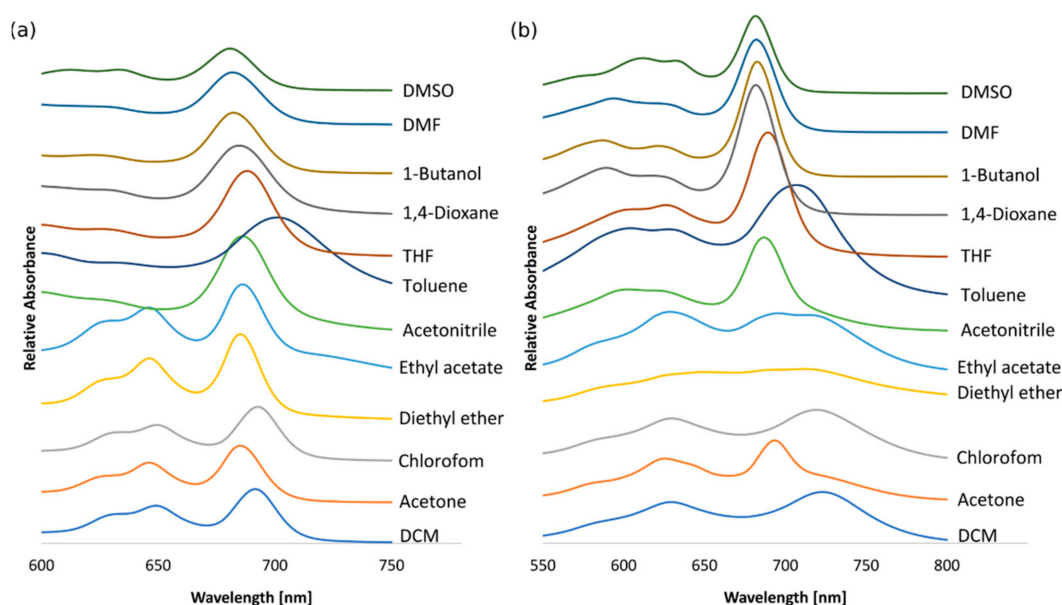
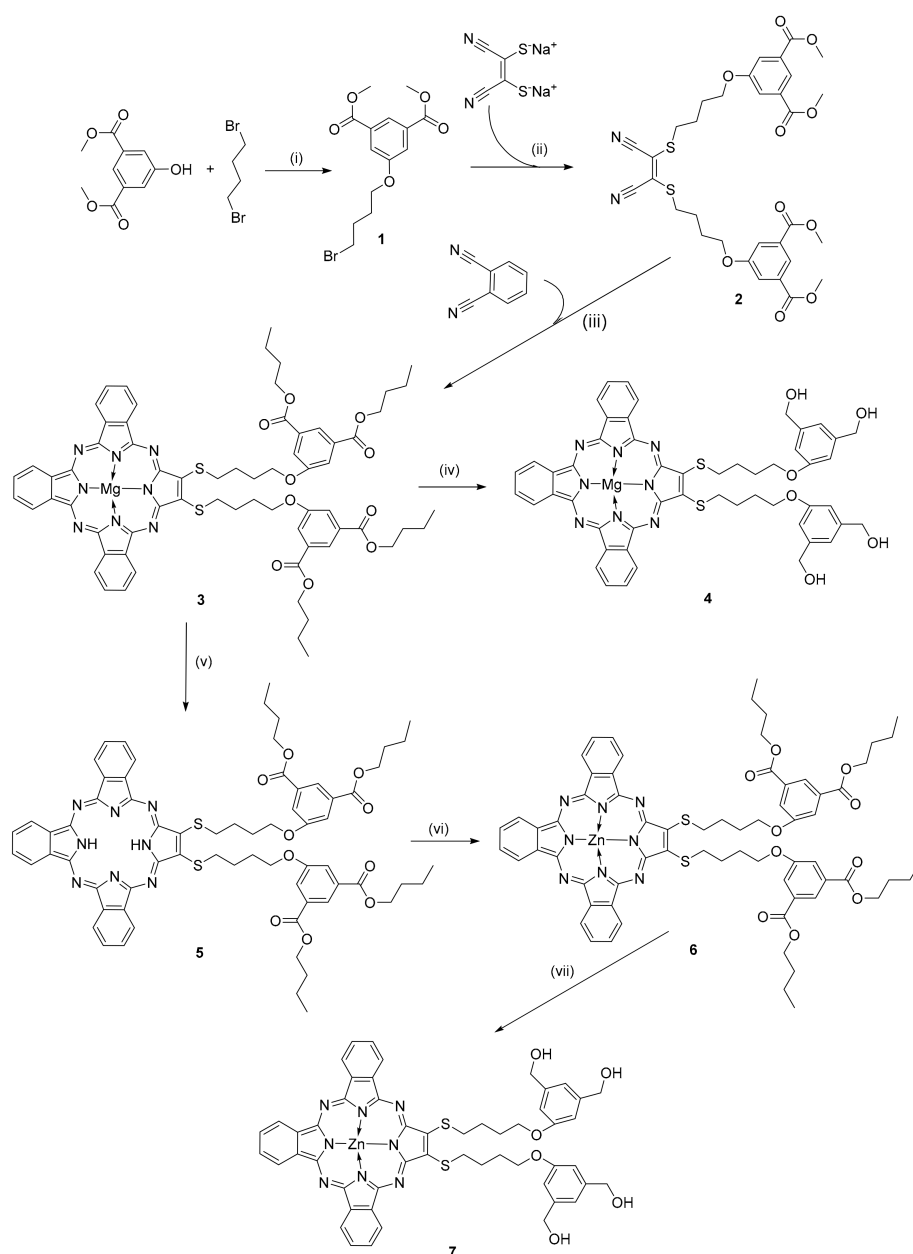


Figure 1. The variation in the Q-band in various solvents for **6** (a) and **7** (b).

Table 1. Soret bands and Q-bands in the UV-Vis spectra of tribenzoporphyrazine derivatives **6** and **7** recorded in various solvents.

SOLVENT	6		7	
	λ_2/nm (Soret Band)	λ_1/nm (Q-Band)	λ_2/nm (Soret Band)	λ_1/nm (Q-Band)
dichloromethane	352	692	358	723
acetone	354	685	356	693
chloroform	353	693	357	719
diethyl ether	353	685	357	713
ethyl acetate	354	686	355	696
acetonitrile	356	686	356	687
toluene	361	701	360	707
thf	355	688	356	689
1,4-dioxane	346	685	357	682
1-butanol	347	682	354	683
dmf	364	682	366	682
dmsO	337	681	338	682



Scheme 1. Reagents and conditions for the synthesis of compounds 1–7: (i) K₂CO₃, DMF, rt, 48 h; (ii) K₂CO₃, DMF, rt, 48 h [20]; (iii) Mg(*n*OC₄H₉)₂, *n*BuOH, reflux, 24 h [20]; (iv) LiAlH₄, THF, 0 °C→rt, 2 h [20]; (v) CF₃COOH, room temperature, 30 min [21]; (vi) (CH₃COO)₂Zn, DMF, 70 °C, 24 h; (vii) LiAlH₄, THF, 0 °C→rt, 40 min; rt—room temperature.

3.3. Solvatochromic Studies

In the UV-Vis spectra of **6** (Figure 1a) and **7** (Figure 1b) recorded in dichloromethane, acetone, chloroform, diethyl ether, and ethyl acetate, intense Q-bands were considerably split into two components. The split was less marked for the other solvents, such as acetonitrile, toluene, THF, 1,4-dioxane, 1-butanol, DMF, and DMSO. Therefore, solvent effects on UV-Vis absorption spectra were studied in selected protic and aprotic solvents. In the Q-band region, depending on the applied solvent, the positions and intensities of the bands were influenced. For **6**, the largest red shift was noted in toluene, whereas the highest blue shift was observed in DMSO. For **7**, the largest red shift was noted in dichloromethane, and the highest blue shift was observed in 1,4-dioxane, DMF, and DMSO.

To evaluate the solvatochromic effects, the correlation between the refractive indices of solvents and Q-band shifts was tested [24,34,35]. The $1/F$ value is a rational function of the solvent's refractive index (n), which is calculated from the equation:

$$F = \frac{n^2 - 1}{2n^2 + 1} \quad (1)$$

The wavelength (λ_{\max} in nm), representing the maximum of the Q-band, was plotted against $1/F$. For tribenzoporphyrzine derivative **6**, the linear correlation characterized by the correlation index (R^2) of 0.86 (Figure 2a) was calculated for 8 out of 12 solvents, such as dichloromethane, acetone, chloroform, diethyl ether, ethyl acetate, acetonitrile, toluene, and THF. For macrocycle **7**, the linear correlation index (R^2) of 0.82 (Figure 2b) was found for the following solvents: diethyl ether, ethyl acetate, THF, 1,4-dioxane, DMF, and DMSO. Notably, the Q-band wavelengths of **6** and **7** in selected solvents were also correlated with the dipole moments. For tribenzoporphyrzine **6**, the linear correlation index (R^2) of 0.91 (Figure 3a) was noted for 6 out of 12 solvents: dichloromethane, acetone, chloroform, toluene, THF, and DMSO. The correlation between the dipole moment of the solvent and the λ_{\max} of the Q-band for compound **7** was calculated as a value of 0.94 (Figure 3b) for solvents such as acetone, ethyl acetate, acetonitrile, toluene, DMF, and DMSO. The outcomes of the solvatochromic study performed for **6** and **7** might suggest that the red shift of the Q-band can be the result of the coordinating strength of the solvent or solvation. The amount of data considered for both plots (Q-band vs. refractive index and Q-band vs. dipole moment) is related to the best R^2 . Adding more solvents decreased the significance of the obtained results. The data used for calculations, i.e., the absorption maxima of **6** and **7** as well as the values of the refractive indices (n_D) and dipole moments (μ) in the applied solvents, are presented in Table 2.

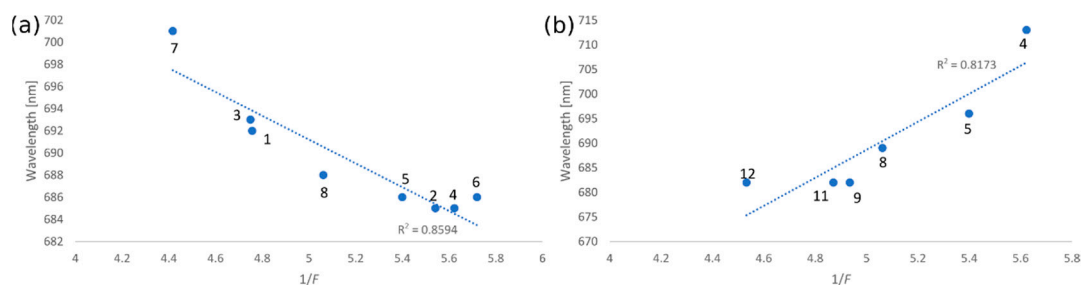


Figure 2. Plots of the wavelength of the Q-band maximum absorbance vs. the rational function of the solvent's refractive index ($1/F$) for **6** (a) and **7** (b). Solvents used: (1) dichloromethane, (2) acetone, (3) chloroform, (4) diethyl ether, (5) ethyl acetate, (6) acetonitrile, (7) toluene, (8) THF, (9) 1,4-dioxane, (10) 1-butanol *, (11) DMF, and (12) DMSO; *—correlation was not found, therefore not added to the figure.

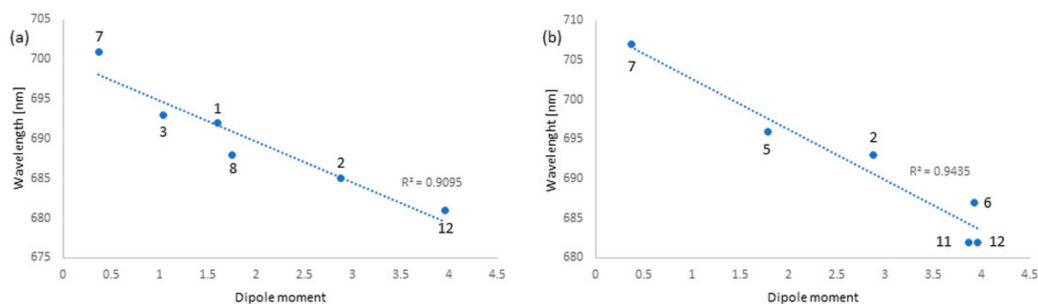


Figure 3. Plots of the wavelength of the Q-band maximum absorbance vs. the dipole moment of solvents for **6** (a) and **7** (b). Solvents used: (1) dichloromethane, (2) acetone, (3) chloroform, (4) diethyl ether *, (5) ethyl acetate, (6) acetonitrile, (7) toluene, (8) THF, (9) 1,4-dioxane *, (10) 1-butanol *, (11) DMF, and (12) DMSO; *—correlation was not found, therefore not added to the figure.

Table 2. The variation in the Q-band for **6** and **7** in different solvents (dipole moments and refractive indexes [24,35]).

Solvent	Refractive Index (n_D)	Dipole Moment (μ)	Q-Band (λ_{max} , nm) 6	Q-Band (λ_{max} , nm) 7
dichloromethane	1.445	1.60	692	723
acetone	1.359	2.88	685	693
chloroform	1.446	1.04	693	719
diethyl ether	1.352	1.15	685	713
ethyl acetate	1.372	1.78	686	696
acetonitrile	1.344	3.92	686	687
toluene	1.497	0.37	701	707
THF	1.407	1.75	688	689
1,4-dioxane	1.422	0	685	682
1-butanol	1.399	1.66	682	683
DMF	1.430	3.82	682	682
DMSO	1.478	3.96	681	682

3.4. Electrochemical Studies

The electrochemical measurements were performed using two zinc(II) tribenzoporphyrzine derivatives, **6** and **7**, to assess their electroactivity towards potential uses as semiconductors or electrocatalysts. The cyclic voltammetry (CV) and differential pulse voltammetry (DPV) studies were applied in the classic three-electrode system with the glassy carbon working electrode, a platinum wire as a counter electrode, and a silver wire as a pseudo-reference. Due to the insolubility of Pzs **6** and **7** in water, the measurements were performed in dichloromethane with the addition of a tetrabutylammonium perchlorate (TBAP) electrolyte (0.1M). Ferrocene was used as an internal standard, and all voltammograms were adjusted to the ferrocenium/ferrocene peak potential. The CV scans were performed in the range of 25–200 mV/s.

In the voltammogram of **6**, two reduction peaks and one oxidation peak were observed in the electrochemical window between -2.0 V and $+1.0$ V. The second oxidation peak was not noted in the CV scans (Figure 4a). However, its evolution was observed at the boundary of the electrochemical window in the DPV scan (Figure 4b). All redox peaks were correlated with the oxidation or reduction of the macrocycle ring due to the presence of the electrochemically inactive zinc(II) cation inside the core.

The CV and DPV studies of **7**, which is a reduced derivative of Pz **6**, revealed four redox peaks: two reductions and two oxidations in the investigated potential window (Figure 5). Within the first reduction peak, an additional descending peak can be observed related to the aggregation phenomenon of the studied porphyrzine, which is commonly observed in the voltammograms of other porphyrinoids in dichloromethane. The electrochemical data of Pzs **6** and **7** are presented in Table 3. A positive shift of 0.1 V of peak potentials for Pz **7** compared to Pz **6** was noticed. It may be a result of replacing electron-withdrawing groups (ester groups) with electron-donating groups (hydroxymethyl groups). In both cases, the electrochemical bandgap, E_{gap} , presented the same value of 1.5 eV.

The obtained electrochemical data for Pz **6** were compared to its symmetrical analogue, an octasubstituted porphyrzine synthesized previously by our group [36], which was previously subjected to CV and DPV measurements in the same conditions as presented here. For the symmetrical zinc(II) sulfanyl porphyrzine with peripheral isophthaloxybutyl-sulfanyl substituents, the first reduction peak occurred at -1.01 V, while the first oxidation was noted at 0.67 V [36]. Considering this data, the redox processes were positively shifted in the symmetrical derivative, and the electrochemical bandgap was slightly higher in comparison to the unsymmetrical macrocycle **6** as a result of the presence of more electron-withdrawing ester groups in the macrocycle. Another example constitutes a symmetrical zinc(II) sulfanyl porphyrzine with (morpholin-4-yl)ethyl peripheral groups, which was

studied in DCM/0.1M TBAP with ferrocene as an internal standard. In this case, the first redox peak was even more positively shifted in comparison to **6** and **7** [37]. However, the absence of aromatic peripheral substituents resulted in a lower electrochemical bandgap, unlike the case of the other macrocycles studied in this paper.

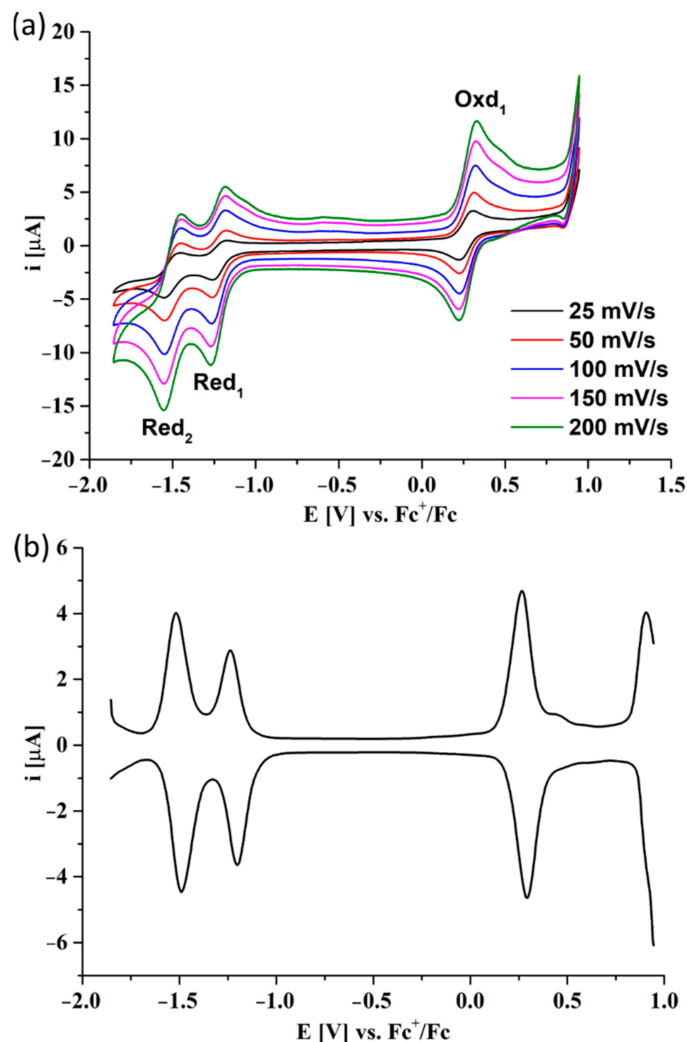


Figure 4. The CV (a) and DPV (b) voltammograms of **6** in DCM/0.1M TBAP. DPV parameters: modulation amplitude 20 mV, step rate $5 \text{ mV} \times \text{s}^{-1}$.

Table 3. The electrochemical data of porphyrazines **6** and **7**.

Pz	Red ₂	Red ₁	Oxd ₁	Oxd ₂	E _{gap}	Ref.
6	−1.50 V	−1.22 V	0.28 V	-	1.50 eV	This work
7	−1.39 V	−1.12 V	0.38 V	0.61 V	1.50 eV	This work
Sym ZnPz ¹	−1.24 V	−1.01 V	0.67 V	-	1.68 eV	[36]
Sym ZnPz ²	−1.34 V	−0.74 V	0.53 V	-	1.27 eV	[37]

¹ 2,3,7,8,12,13,17,18–octakis[4-(3,5-dibutoxycarbonylphenoxy)butylthio]porphyrazinato zinc(II). ² 2,3,7,8,12,13,17,18–octakis[2-(morpholin-4-yl)ethylsulfanyl]porphyrazinato zinc(II).

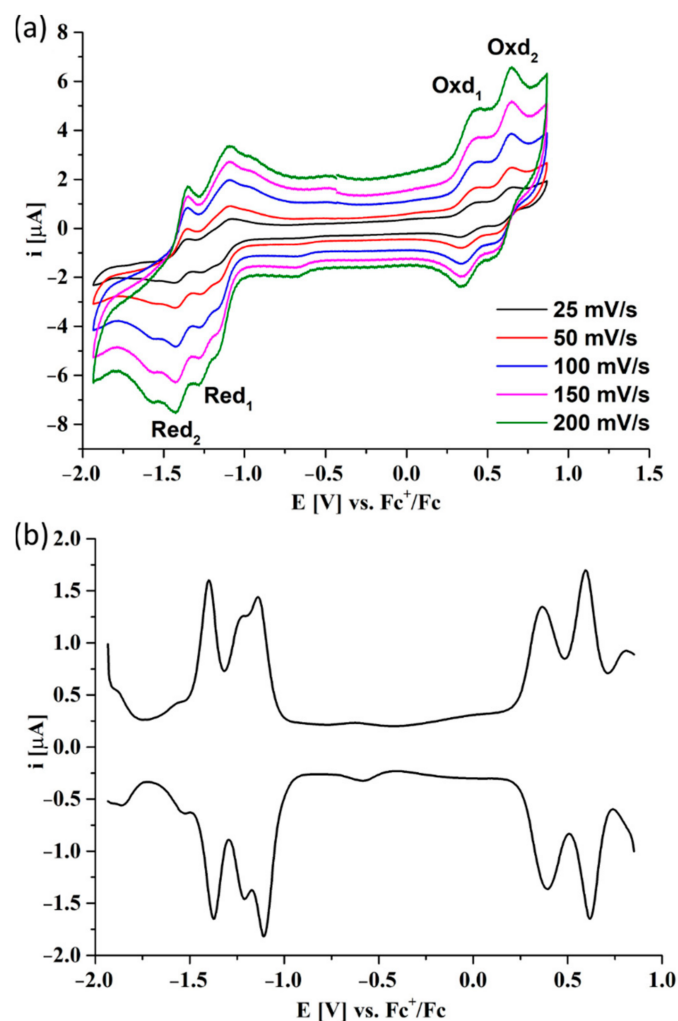


Figure 5. The CV (a) and DPV (b) voltammograms of 7 in DCM/0.1M TBAP. DPV parameters: modulation amplitude 20 mV, step rate $5 \text{ mV} \times \text{s}^{-1}$.

What is more, all oxidation and reduction processes in 6 (Figure 6a) and 7 (Figure 6b) are diffusion-controlled due to a linear correlation of the peak currents of the redox pairs versus the square root scan rate.

3.5. Singlet Oxygen Generation Study

To assess the potential application of the new tribenzoporphyrazines in photodynamic therapy, the quantum yields of singlet oxygen generation in DMSO were measured spectrophotometrically using an indirect method with 1,3-diphenylisobenzofuran (DPBF). DPBF is a compound that easily reacts with singlet oxygen, with a breakage of furan ring, and its peak at about 400 nm decreases over time (Figures 7 and 8) as it decomposes. The changes in absorption were then calculated to give singlet oxygen quantum yields (Φ_{Δ}). As a reference, zinc(II) phthalocyanine was used. Compound 6 generated oxygen with a quantum yield value of 0.24, which indicates the moderate photosensitizing potential, whereas 7 presented an even higher quantum yield, reaching the value of 0.59. The measured singlet oxygen generation values can be considered as high compared to those previously obtained for the studied magnesium(II) 3 and 4 analogs and other porphyrazine derivatives presented in the literature (Table 4). It was found by Gierszewski et al. [38] that porphyrazines with eight peripheral isophthaloxylalkylsulfanyl substituents generate singlet oxygen with Φ_{Δ} values between 0.01 and 0.04 in DMF and that incorporating Mg^{2+} ions into the Pzs improves their capability to generate single oxygen. The exchange of Mg^{2+} (3, 6) to Zn^{2+} (4, 7) in the tribenzoporphyrazine ring influenced the singlet oxygen generation

quantum yield values, which increased from 0.05 (3) to 0.24 (4) and from 0.20 (6) to 0.59 (7). In Figures 7 and 8, the Q-bands of 6 and 7 demonstrate only minimal to no changes during irradiation, thus indicating their good stability during measurements.

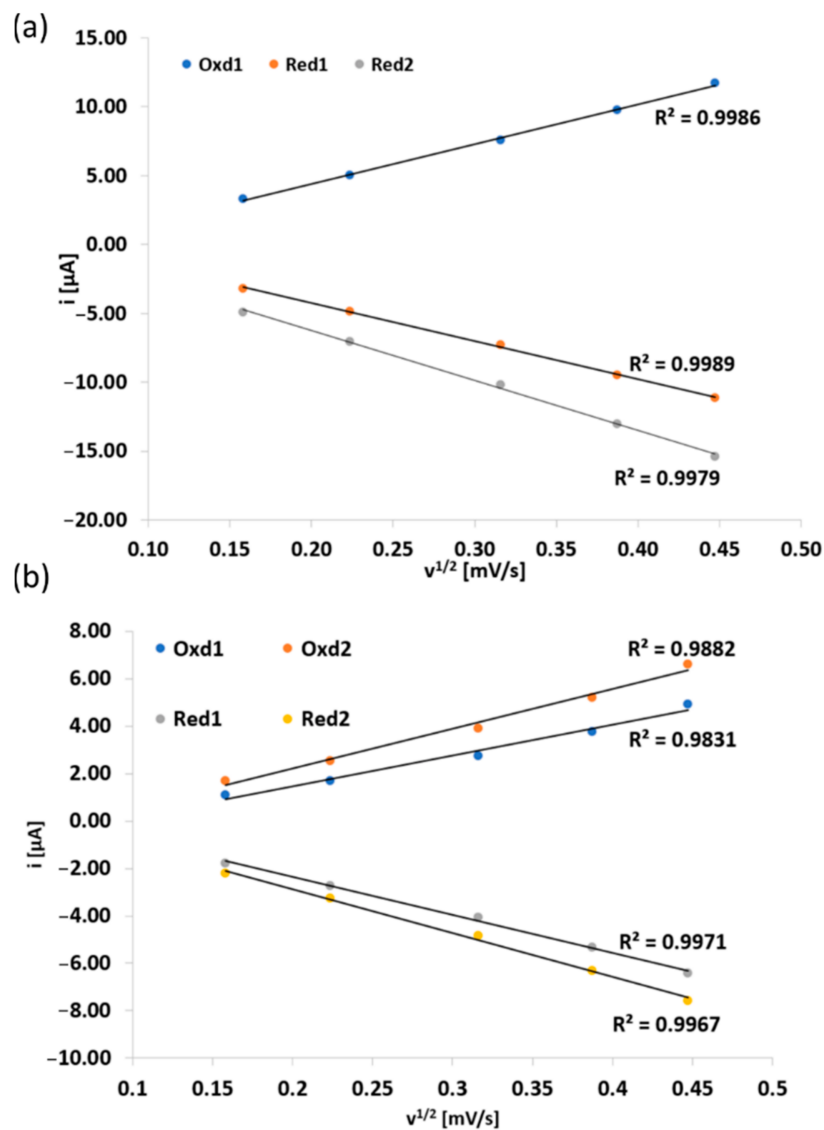


Figure 6. Peak current vs. square root scan rate for redox peaks of Pzs 6 (a) and 7 (b).

Table 4. Quantum yields of singlet oxygen generation by Pzs 3, 4, 6, and 7 in DMSO.

PZ	SINGLET OXYGEN GENERATION	
	Singlet oxygen quantum yield [Φ_{Δ}] ^[a]	
3 [20]	0.05	
4 [20]	0.20	
6	0.24	
7	0.59	

^[a] error ≤ 0.01

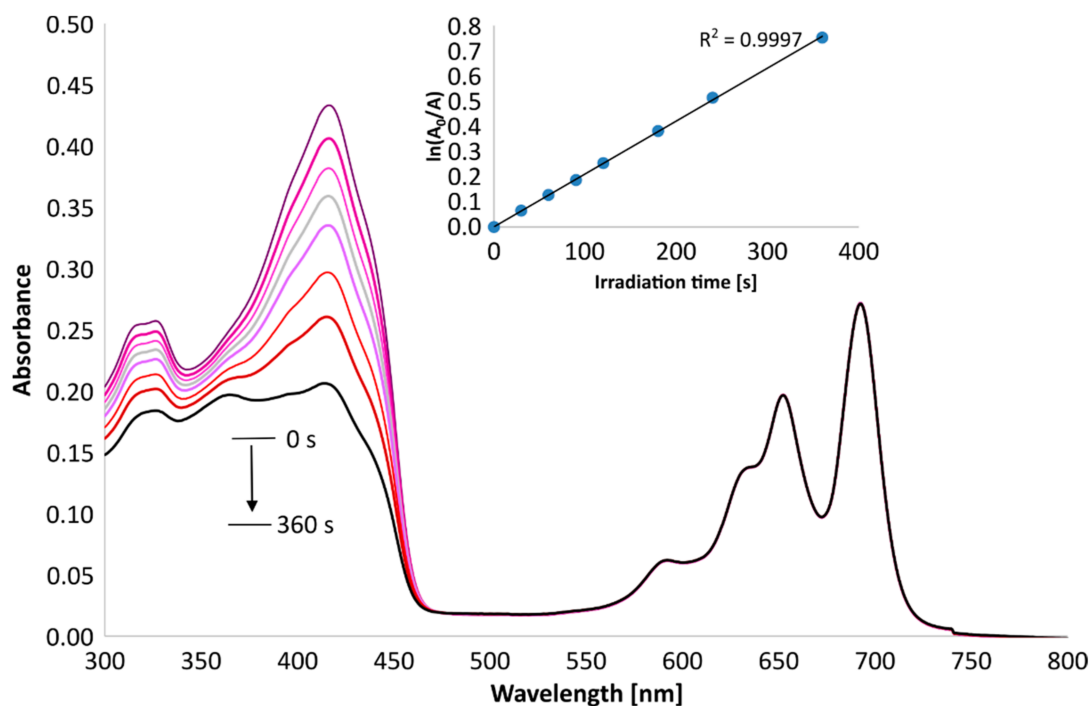


Figure 7. Changes in the UV-Vis spectrum of 6 and DPBF mixture in DMSO during irradiation at 665 nm.

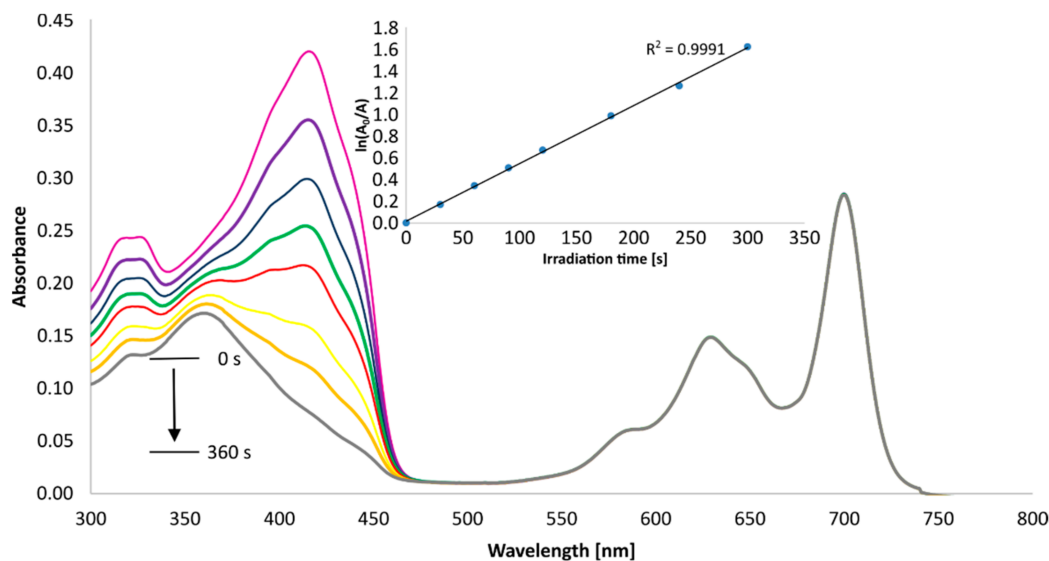


Figure 8. Changes in the UV-Vis spectrum of 7 and DPBF mixture in DMSO during irradiation at 665 nm.

3.6. Ecotoxicity Assessment

In the acute toxicity test, the changes in bioluminescence are correlated with *Aliivibrio fischeri* bacterial metabolism. The luminescence linearly decreases with the increasing toxicity of an added sample. Compounds 4 and 6 induced no changes in the cell viability after exposure to red light in comparison to dark conditions, as can be seen in Figure 9. Quite the opposite effect can be observed for 3 and 7, in which case the cell viability was lower after irradiation. On the other hand, the values obtained for 3 present much higher variability, which suggests that they should be treated with caution. Additionally, such results are somewhat unusual, as they cannot be associated with higher singlet oxygen generation yields (Table 4). However, it can be seen that in all cases the higher concentration

of the macrocycles (10^{-4} M) induced dark toxicity. Based on the results obtained earlier for the magnesium derivatives on bacterial strains and cancer cell lines [20,39], this toxic effect was probably caused by the absorption of the emitted bacterial bioluminescence at 490 nm by the macrocycles or was a result of the specificity of the test.

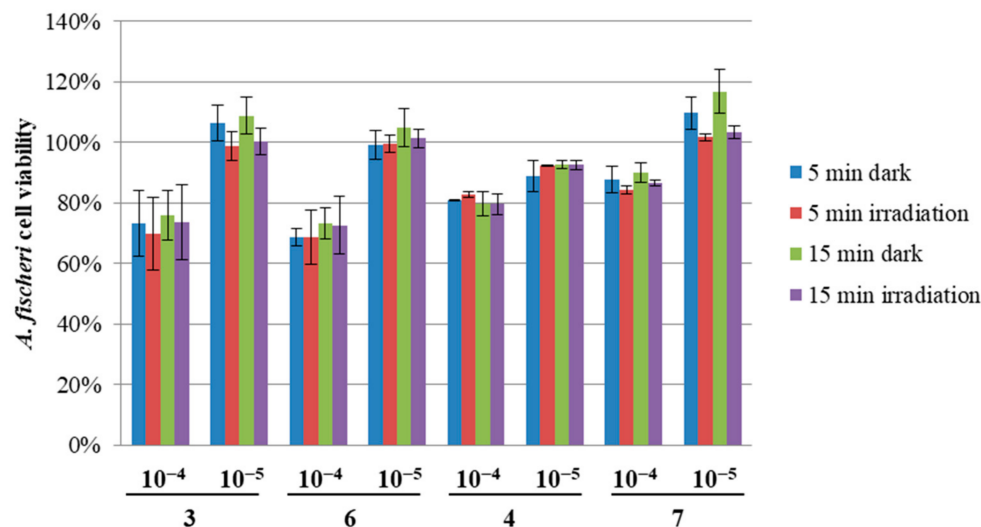


Figure 9. Changes in the *Aliivibrio fischeri* cell viability upon exposure to the tested porphyrazines 3, 4, 6, and 7 at 10^{-4} or 10^{-5} concentrations.

4. Conclusions

In summary, two new zinc(II) tribenzoporphyrazines with sulfanyl substituents were obtained and subjected to various photophysical measurements as well as an initial acute toxicity assessment. The results were compared to their magnesium(II)-containing counterparts. The synthesis started from obtaining a maleonitrile derivative according to the published procedure, then using this compound and the excess of 1,2-dicyanobenzene in Linstead's macrocyclization reaction conditions resulted in the formation of magnesium(II) tribenzoporphyrazine with 4-(3,5-dibutoxycarbonylphenoxy)butylthio substituents. Next, the magnesium derivative was demetallated with trifluoroacetic acid and subsequently remetallated with zinc(II) acetate toward zinc(II) tribenzoporphyrazine. The next step of the synthesis was the peripheral modification, as zinc(II) tribenzoporphyrazines was subjected to a reduction reaction with LiAlH_4 , which led to zinc(II) tribenzoporphyrazine with 4-[3,5-di(hydroxymethyl)phenoxy]butylthio substituents. The new zinc(II) tribenzoporphyrazines were characterized by UV-Vis spectroscopy, various NMR techniques (^1H NMR, ^{13}C NMR, ^1H - ^1H COSY, ^1H - ^{13}C HSQC, and ^1H - ^{13}C HMBC), and mass spectrometry. The UV-Vis spectra of the new macrocycles were recorded in different solvents and subjected to a solvatochromic study in which the positions of the Q-bands of each solvent were analyzed. Both macrocycles were studied using electrochemical measurements. In the voltammogram of zinc(II) tribenzoporphyrazine with 4-(3,5-dibutoxycarbonylphenoxy)butylthio substituents, two reduction peaks and one oxidation peak were observed in the electrochemical window between -2.0 V and $+1.0$ V, whereas the second oxidation peak was not noted in the CV scans. The evolution of this peak was observed at the boundary of the electrochemical window in the DPV scan. The CV and DPV studies of zinc(II) tribenzoporphyrazine with 4-[3,5-di(hydroxymethyl)phenoxy]butylthio substituents revealed four redox peaks: two reductions and two oxidations in the analyzed potential window. The electrochemical bandgap, E_{gap} , of both zinc(II) tribenzoporphyrazines presented the same value of 1.5 eV. What is more, all oxidation and reduction processes for both macrocycles were diffusion-controlled due to a linear correlation of the peak currents of the redox pairs versus the square root scan rate. In the photochemical assessment of the singlet oxygen generation, both zinc(II) tribenzoporphyrazines revealed moderate to high quantum yield generation values of 0.24 and 0.59 in DMSO. The results of the Microtox[®] bioluminescence

assay showed that the newly obtained zinc(II) macrocycles can be regarded as potential photosensitizers for further applications in medicine, while the electrochemical assessment proved that these molecules may be regarded as useful for new technology development.

Supplementary Materials: The following are available online at <https://www.mdpi.com/article/10.3390/app12136825/s1>. Figure S1. NMR data of **6**: ^1H and (^{13}C) chemical shift values [ppm] and key correlations observed in NMR spectra. Bold lines: ^1H - ^1H COSY; Arrows: ^1H - ^{13}C HMBC. Figure S2. NMR data of **7**: ^1H and (^{13}C) chemical shift values [ppm] and key correlations observed in NMR spectra. Bold lines: ^1H - ^1H COSY; Arrows: ^1H - ^{13}C HMBC. Table S1. ^1H and ^{13}C NMR data obtained for **6** including key correlations determined from ^1H - ^1H COSY, ^1H - ^{13}C HSQC and ^1H - ^{13}C HMBC spectra. Table S2. ^1H and ^{13}C NMR data obtained for **7** including key correlations determined from ^1H - ^1H COSY, ^1H - ^{13}C HSQC and ^1H - ^{13}C HMBC spectra.

Author Contributions: Conceptualization, P.K. and T.G.; methodology, P.K., T.K. and D.T.M.; formal analysis, P.K., T.K. and D.T.M.; investigation, P.K., T.K. and D.T.M.; resources, T.G.; data curation, P.K.; writing—original draft preparation, P.K., T.K. and D.T.M.; writing—review and editing, P.K. and T.G.; supervision, T.G. and T.K.; project administration, T.G.; funding acquisition, T.G. All authors have read and agreed to the published version of the manuscript.

Funding: This research was funded by the National Science Centre, Poland, within grant No. 2020/39/O/NZ7/00351.

Institutional Review Board Statement: Not applicable.

Informed Consent Statement: Not applicable.

Data Availability Statement: All the data produced in this study is contained in the manuscript text.

Conflicts of Interest: The authors declare no conflict of interest.

References

1. Rodríguez-Morgade, M.S.; Stuzhin, P.A. The Chemistry of Porphyrazines: An Overview. *J. Porphyr. Phthalocyanines* **2004**, *8*, 1129–1165. [[CrossRef](#)]
2. Zong, H.; Sun, P.; Mirkin, C.A.; Barrett, A.G.M.; Hoffman, B.M. Varying the Electrochemical Potential and Thickness of Porphyrazine SAMs by Molecular Design. *J. Phys. Chem. B* **2009**, *113*, 14892–14903. [[CrossRef](#)] [[PubMed](#)]
3. Motyka, M.; Steer, R.P.; Williams, C.C.; Lee, S.; Ghiggino, K.P. Concerning the Dual Emission of Porphyrazines Employed in Biomedical Imaging. *Photochem. Photobiol. Sci.* **2013**, *12*, 1086. [[CrossRef](#)] [[PubMed](#)]
4. Miletin, M.; Zimcik, P.; Novakova, V. Photodynamic Properties of Aza-Analogues of Phthalocyanines. *Photochem. Photobiol. Sci.* **2018**, *17*, 1749–1766. [[CrossRef](#)] [[PubMed](#)]
5. Novakova, V.; Donzello, M.P.; Ercolani, C.; Zimcik, P.; Stuzhin, P.A. Tetrapyrizinoporphyrazines and Their Metal Derivatives. Part II: Electronic Structure, Electrochemical, Spectral, Photophysical and Other Application Related Properties. *Coord. Chem. Rev.* **2018**, *361*, 1–73. [[CrossRef](#)]
6. Dąbrowski, J.M.; Pucelik, B.; Regiel-Futyra, A.; Brindell, M.; Mazuryk, O.; Kyziół, A.; Stochel, G.; Macyk, W.; Arnaut, L.G. Engineering of Relevant Photodynamic Processes through Structural Modifications of Metallotetrapyrrolic Photosensitizers. *Coord. Chem. Rev.* **2016**, *325*, 67–101. [[CrossRef](#)]
7. Zhou, Z.; Zhang, L.; Zhang, Z.; Liu, Z. Advances in Photosensitizer-Related Design for Photodynamic Therapy. *Asian J. Pharm. Sci.* **2021**, *16*, 668–686. [[CrossRef](#)]
8. O'Connor, A.E.; Gallagher, W.M.; Byrne, A.T. Porphyrin and Nonporphyrin Photosensitizers in Oncology: Preclinical and Clinical Advances in Photodynamic Therapy. *Photochem. Photobiol.* **2009**, *85*, 1053–1074. [[CrossRef](#)]
9. Agostinis, P.; Berg, K.; Cengel, K.A.; Foster, T.H.; Girotti, A.W.; Gollnick, S.O.; Hahn, S.M.; Hamblin, M.R.; Juzeniene, A.; Kessel, D.; et al. Photodynamic Therapy of Cancer: An Update. *CA Cancer J. Clin.* **2011**, *61*, 250–281. [[CrossRef](#)]
10. Stolarska, M.; Glowacka-Sobotta, A.; Ziental, D.; Długaszewska, J.; Falkowski, M.; Goslinski, T.; Sobotta, L. Photochemical Properties and Promising Activity against Staphylococci of Sulfanyl Porphyrazines with Dendrimeric Moieties. *Inorg. Chim. Acta* **2021**, *521*, 120321. [[CrossRef](#)]
11. Skupin-Mrugalska, P.; Piskorz, J.; Goslinski, T.; Mielcarek, J.; Konopka, K.; Düzgüneş, N. Current Status of Liposomal Porphyrinoid Photosensitizers. *Drug Discov. Today* **2013**, *18*, 776–784. [[CrossRef](#)] [[PubMed](#)]
12. Piskorz, J.; Mlynarczyk, D.T.; Szczolko, W.; Konopka, K.; Düzgüneş, N.; Mielcarek, J. Liposomal Formulations of Magnesium Sulfanyl Tribenzoporphyrazines for the Photodynamic Therapy of Cancer. *J. Inorg. Biochem.* **2018**, *184*, 34–41. [[CrossRef](#)] [[PubMed](#)]

13. Sobotta, L.; Długaszewska, J.; Kasprzycki, P.; Lijewski, S.; Teubert, A.; Mielcarek, J.; Gdaniec, M.; Goslinski, T.; Fita, P.; Tykarska, E. In Vitro Photodynamic Activity of Lipid Vesicles with Zinc Phthalocyanine Derivative against *Enterococcus Faecalis*. *J. Photochem. Photobiol. B Biol.* **2018**, *183*, 111–118. [[CrossRef](#)]
14. Darwish, W. Polymers for Enhanced Photodynamic Cancer Therapy: Phthalocyanines as a Photosensitizer Model. *Polym. Adv. Technol.* **2020**, *32*, 919–930. [[CrossRef](#)]
15. Shilyagina, N.Y.; Peskova, N.N.; Lermontova, S.A.; Brilkina, A.A.; Vodeneev, V.A.; Yakimansky, A.V.; Klapshina, L.G.; Balalaeva, I.V. Effective Delivery of Porphyrine Photosensitizers to Cancer Cells by Polymer Brush Nanocontainers. *J. Biophoton.* **2017**, *10*, 1189–1197. [[CrossRef](#)] [[PubMed](#)]
16. Thakur, N.S.; Mandal, N.; Patel, G.; Kirar, S.; Reddy, Y.N.; Kushwah, V.; Jain, S.; Kalia, Y.N.; Bhaumik, J.; Banerjee, U.C. Co-Administration of Zinc Phthalocyanine and Quercetin via Hybrid Nanoparticles for Augmented Photodynamic Therapy. *Nanomed. Nanotechnol. Biol. Med.* **2021**, *33*, 102368. [[CrossRef](#)]
17. Lucky, S.S.; Soo, K.C.; Zhang, Y. Nanoparticles in Photodynamic Therapy. *Chem. Rev.* **2015**, *115*, 1990–2042. [[CrossRef](#)]
18. Lijewski, S.; Gierszewski, M.; Sobotta, L.; Piskorz, J.; Kordas, P.; Kucinska, M.; Baranowski, D.; Gdaniec, Z.; Murias, M.; Karolczak, J.; et al. Photophysical Properties and Photochemistry of a Sulfanyl Porphyrine Bearing Isophthaloxybutyl Substituents. *Dye. Pigment.* **2015**, *113*, 702–708. [[CrossRef](#)]
19. Klein, T.; Ziegler, T. First Example of an Octa-Glycoconjugated Magnesium(II)Porphyrine. *Tetrahedron Lett.* **2016**, *57*, 495–497. [[CrossRef](#)]
20. Mlynarczyk, D.T.; Lijewski, S.; Falkowski, M.; Piskorz, J.; Szczolko, W.; Sobotta, L.; Stolarska, M.; Popena, L.; Jurga, S.; Konopka, K.; et al. Dendrimeric Sulfanyl Porphyrines: Synthesis, Physico-Chemical Characterization, and Biological Activity for Potential Applications in Photodynamic Therapy. *ChemPlusChem* **2016**, *81*, 460–470. [[CrossRef](#)]
21. Mlynarczyk, D.T.; Piskorz, J.; Popena, L.; Stolarska, M.; Szczolko, W.; Konopka, K.; Jurga, S.; Sobotta, L.; Mielcarek, J.; Düzgüneş, N.; et al. S-Seco-Porphyrine as a New Member of the Seco-Porphyrine Family—Synthesis, Characterization and Photocytotoxicity against Cancer Cells. *Bioorg. Chem.* **2020**, *96*, 103634. [[CrossRef](#)] [[PubMed](#)]
22. Sobotta, L.; Fita, P.; Szczolko, W.; Wrotyński, M.; Wierzchowski, M.; Goslinski, T.; Mielcarek, J. Functional Singlet Oxygen Generators Based on Porphyrines with Peripheral 2,5-Dimethylpyrrol-1-yl and Dimethylamino Groups. *J. Photochem. Photobiol. A Chem.* **2013**, *269*, 9–16. [[CrossRef](#)]
23. Seotsanyana-Mokhosi, I.; Kuznetsova, N.; Nyokong, T. Photochemical Studies of Tetra-2,3-Pyridinoporphyrines. *J. Photochem. Photobiol. A Chem.* **2001**, *140*, 215–222. [[CrossRef](#)]
24. Ogunsipe, A.; Maree, D.; Nyokong, T. Solvent Effects on the Photochemical and Fluorescence Properties of Zinc Phthalocyanine Derivatives. *J. Mol. Struct.* **2003**, *650*, 131–140. [[CrossRef](#)]
25. Chelminiak-Dudkiewicz, D.; Rybczynski, P.; Smolarkiewicz-Wyczachowski, A.; Mlynarczyk, D.T.; Wegrzynowska-Drzymalska, K.; Ilnicka, A.; Goslinski, T.; Marszał, M.P.; Ziegler-Borowska, M. Photosensitizing Potential of Tailored Magnetite Hybrid Nanoparticles Functionalized with Levan and Zinc(II) Phthalocyanine. *Appl. Surf. Sci.* **2020**, *524*, 146602. [[CrossRef](#)]
26. Linstead, R.P.; Whalley, M. 944. Conjugated Macrocycles. Part XXII. Tetraporphin and Its Metallic Derivatives. *J. Chem. Soc.* **1952**, 4839–4846. [[CrossRef](#)]
27. Montalban, A.G.; Lange, S.J.; Beall, L.S.; Mani, N.S.; Williams, D.J.; White, A.J.P.; Barrett, A.G.M.; Hoffman, B.M. Seco-Porphyrines: Synthetic, Structural, and Spectroscopic Investigations. *J. Org. Chem.* **1997**, *62*, 9284–9289. [[CrossRef](#)]
28. Höger, S. Methoxycarbonyl-Terminated Dendrons via the Mitsunobu Reaction: An Easy Way to Functionalized Hyperbranched Building Blocks. *Synthesis* **1997**, 1997, 20–22. [[CrossRef](#)]
29. Nostrum van, C.F.; Benneker, F.B.G.; Brussaard, H.; Kooijman, H.; Veldman, N.; Spek, A.L.; Schoonman, J.; Feiters, M.C.; Nolte, R.J.M. Dithiacrown Ether Substituted Porphyrines: Synthesis, Single-Crystal Structure, and Control of Aggregation in Solution by Complexation of Transition-Metal Ions. *Inorg. Chem.* **1996**, *35*, 959–969. [[CrossRef](#)]
30. Sibert, J.W.; Baumann, T.F.; Williams, D.J.; White, A.J.P.; Barrett, A.G.M.; Hoffman, B.M. Gemini-Porphyrines: The Synthesis and Characterization of Metal-Capped *Cis*- and *Trans* -Porphyrine Tetrathiolates. *J. Am. Chem. Soc.* **1996**, *118*, 10487–10493. [[CrossRef](#)]
31. Araújo, A.R.L.; Tomé, A.C.; Santos, C.I.M.; Faustino, M.A.F.; Neves, M.G.P.M.S.; Simões, M.M.Q.; Moura, N.M.M.; Abu-Orabi, S.T.; Cavaleiro, J.A.S. Azides and Porphyrinoids: Synthetic Approaches and Applications. Part 2—Azides, Phthalocyanines, Subphthalocyanines and Porphyrines. *Molecules* **2020**, *25*, 1745. [[CrossRef](#)] [[PubMed](#)]
32. Pereira, G.F.M.; Tasso, T.T. From Cuvette to Cells: How the Central Metal Ion Modulates the Properties of Phthalocyanines and Porphyrines as Photosensitizers. *Inorg. Chim. Acta* **2021**, *519*, 120271. [[CrossRef](#)]
33. Salvati, A.; Ristori, S.; Pietrangeli, D.; Oberdisse, J.; Calamai, L.; Martini, G.; Ricciardi, G. Insertion of a Magnesium(II)-Octacarboranyl(Hexylsulfanyl) Porphyrine into Liposomes: A Physico-Chemical Study. *Biophys. Chem.* **2007**, *131*, 43–51. [[CrossRef](#)] [[PubMed](#)]
34. Bayliss, N.S. The Effect of the Electrostatic Polarization of the Solvent on Electronic Absorption Spectra in Solution. *J. Chem. Phys.* **1950**, *18*, 292–296. [[CrossRef](#)]
35. Chemical Rubber Company. *CRC Handbook of Chemistry and Physics: A Ready-Reference Book of Chemical and Physical Data*, 78th ed.; Lide, D.R., Ed.; Edition 1997–1998; CRC Press: Boca Raton, FL, USA, 1997; ISBN 978-0-8493-0478-1.

36. Rebis, T.; Lijewski, S.; Nowicka, J.; Popenda, L.; Sobotta, L.; Jurga, S.; Mielcarek, J.; Milczarek, G.; Goslinski, T. Electrochemical Properties of Metallated Porphyrazines Possessing Isophthaloxybutylsulfanyl Substituents: Application in the Electrocatalytic Oxidation of Hydrazine. *Electrochim. Acta* **2015**, *168*, 216–224. [[CrossRef](#)]
37. Koczorowski, T.; Szczolko, W.; Teubert, A.; Goslinski, T. Sulfanyl Porphyrazines with Morpholinylethyl Periphery—Synthesis, Electrochemistry, and Photocatalytic Studies after Deposition on Titanium(IV) Oxide P25 Nanoparticles. *Molecules* **2021**, *26*, 2280. [[CrossRef](#)]
38. Gierszewski, M.; Falkowski, M.; Sobotta, L.; Stolarska, M.; Popenda, L.; Lijewski, S.; Wicher, B.; Burdzinski, G.; Karolczak, J.; Jurga, S.; et al. Porphyrazines with Peripheral Isophthaloxyalkylsulfanyl Substituents and Their Optical Properties. *J. Photochem. Photobiol. A Chem.* **2015**, *307*, 54–67. [[CrossRef](#)]
39. Mlynarczyk, D.T.; Długaszewska, J.; Falkowski, M.; Popenda, L.; Kryjewski, M.; Szczolko, W.; Jurga, S.; Mielcarek, J.; Goslinski, T. Tribenzoporphyrazines with Dendrimeric Peripheral Substituents and Their Promising Photocytotoxic Activity against *Staphylococcus Aureus*. *J. Photochem. Photobiol. B Biol.* **2020**, *204*, 111803. [[CrossRef](#)]